Publication date: 2021, january 14th

The book,
"PEROVSKITES AND OTHER FRAMEWORK STRUCTURE MATERIALS
(2D-perovskites, Aurivillius, Ruddlesden-Popper, Dion-Jacobson phases, tungsten bronzes, clays, and others)

New trends and perspectives"

(editors P. Saint-Grégoire and M.B Smirnov)

Is a collective volume of 800 pages with **76 authors** and **26 chapters** on recent developments and hot subjects, divided into two parts:

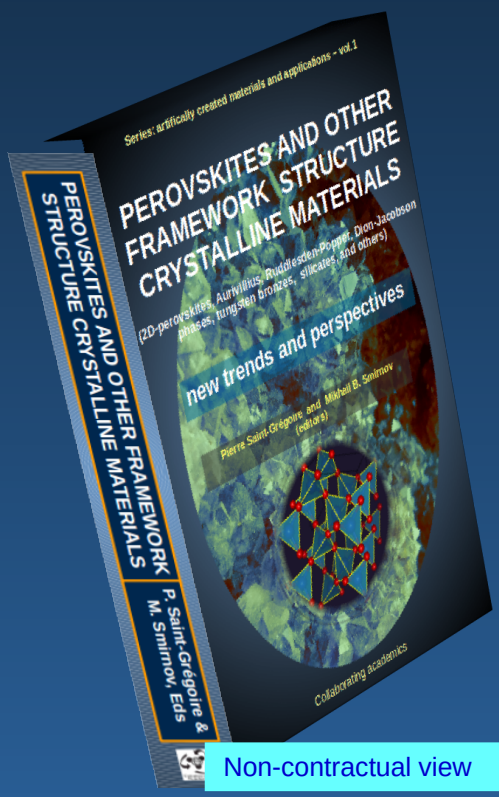

Non-contractual view

A. Fundamental aspects and general properties

B. Elaborated materials and applied properties

Available in 3 formats:

- **Ebook**
- **printed softcover, black & white**
- **printed hardcover, color.**

Go to the Book(click)

Chap. 13 : Influence of the PbO-excess on the structural, microstructural and ferroelectric properties of PLZT ceramics

A.C. Silva [(1)], Y. Mendez-González [(2)], E.C. Lima [(3)], J.D.S. Guerra [(1)]

(1) Grupo de Ferroelétricos e Materiais Multifuncionais, Instituto de Física, Universidade Federal de Uberlândia, Brazil

(2) Facultad de Física-Instituto de Ciencia y Tecnología de Materiales, Universidad de La Habana, Cuba

(3) Universidade Federal do Tocantins, Porto Nacional, Brazil

Corresponding author: santos@ufu.br

Abstract: The physical properties of lead lanthanum zirconate titanate (PLZT) ceramics have been investigated as a function of a PbO excess from 0 to 20 mol% in samples of $Pb_{0.94}La_{0.06}(Zr_{0.6895}Ti_{0.2955})O_3$ (composition that reveals the best performance for piezoelectric applications for materials with rhombohedral symmetry). Results are presented in a compressive way in the frame of an overview on PLZT. Structural, microstructural and ferroelectric properties were investigated as a function of the PbO content. The X-ray diffraction results confirmed the formation of the perovskite structure for all the cases. However, the presence of the Pb_2O_3 secondary phase has been observed for the sample containing 15 mol% PbO excess. Raman spectroscopy studies revealed a strong influence of the PbO content on the active modes shifts. The ferroelectric properties have shown a decrease of both remnant (P_R) and saturation (P_S) polarizations for compositions up to 10 mol% PbO, whereas an increase of P_R and P_S was observed for the higher PbO content samples. Results reveal the effect of the PbO excess on the long-range order interactions for the studied system.

Keywords : FERROELECTRICS, PLZT CERAMICS, PBO-EXCESS, STRUCTURAL PROPERTIES

Cite this paper: A.C. Silva, Y. Mendez-González, E.C. Lima, J.D.S. Guerra, OAJ Materials and Devices, vol 5(2) – chap No13 in "*Perovskites and other Framework Structure Crystalline Materials", p405* (Coll. Acad. 2021) – DOI:10.23647/ca.md20201806

I. Introduction

Lead zirconate titanate [$Pb(Zr_{1-y}Ti_y)O_3$, PZT] ceramics are well-known high-performance piezoelectric materials, which are widely used in sensors, actuators, ferroelectric random access memories (FeRAMs) and dynamic random access memory (DRAM) [1–3]. The piezoelectric, elastic and dielectric properties of this system are improved near the morphotropic phase boundary (MPB), around y = 0.45~0.50, where both rhombohedral (Zr-rich) and tetragonal (Ti-rich) ferroelectric phases coexist [2]. Several studies on X-ray diffraction have been reported over the MPB region, showing a broad not well-defined boundary whose extension strongly depends on the compositional homogeneity as well as the sample processing conditions [4–7]. Figure 1 shows the temperature-composition phase diagram for PZT solid-solution compositions [8].

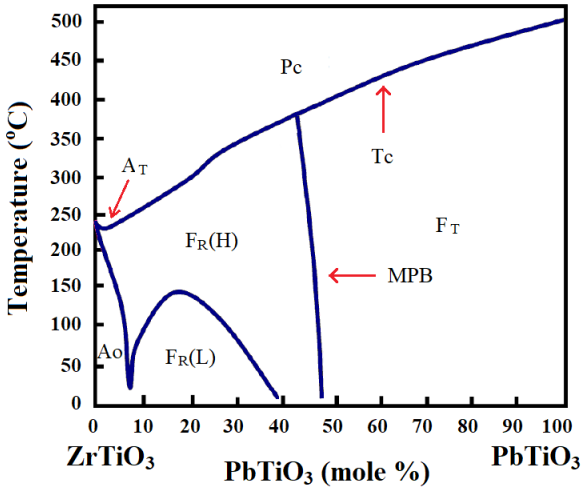

Figure 1: Phase diagram for the $Pb(Zr,Ti)O_3$ solid-solution system [8]. F, A and P represent the ferroelectric, antiferroelectric and paraelectric phases, respectively.

The T_C-line indicates the boundary between the cubic paraelectric (P_C) and tetragonal and rhombohedral (F_T and F_R, respectively) ferroelectric phases. An orthorhombic antiferroelectric (A_O) phase is revealed for compositions $x \leq 6$, from room temperature up to ~200 °C, with no observable piezoelectric effect. In the rhombohedral phase, on the Zr-rich side, the temperature-composition dependence divides this region into two

parts: high F_R(H) and low F_R(L) temperature regions, with R3*m* and R3*c* space groups, respectively. The difference between these two rhombohedral ferroelectric phases is a small lattice distortion that occur in the unit-cell along the [111] crystallographic direction for the R3*c* phase [9]. The tetragonal antiferroelectric (A_T) phase is also represented for very small Ti amount compositions.

The piezoelectric properties (*d* and *k* factors), for composition close to the MBP, are determined by the proximity of maximum permittivity and remnant polarization (P_R), according to the relationships reported by Heywang et al. [10]. A systematic study on the dielectric and piezoelectric properties was in this case carried out for $Pb(Zr_{1-y}Ti_y)O_3$ compounds in the compositional range of the MBP, showing enhanced responses for those compositions [10]. In this way, have been considered fundamental parameters such as: d_{33} - piezoelectric coefficient, which is an indicator of the material deformation along the [001] crystallographic direction when an electric field is applied along the same direction; g_{33} - relates the applied voltage with the generated electric field, which are indicated with the first and second subscript, respectively; k_p - electromechanical coupling factor, that indicates the efficiency with which a piezoelectric material converts electrical energy into mechanical energy, or vice versa; S_m - the large-signal unidirectional strain in the material along *m*-evenly distributed direction. For this system, a piezoelectric coefficient (d_{33}) in the range of 200–600 pC/N has been reported close to the MPB compound [10, 11]. On the other hand, both k_p and S_m factors reach a maximum value for the Ti concentration of y = 0.465 at room temperature [10]. The ferroelectric properties have also been reported by Heywang et al. [10], showing a performance of the remnant polarization (P_R) for the composition with y = 0.44. From the fundamental point of view, P_R represents the polarization that remains in the material once the electric field is removed. The d_{33} values reported for PZT compounds remain still higher than those reached for some lead free $Bi_{0.5}Na_{0.5}TiO_3$-based (120–180 pC/N) and $Bi_{0.5}K_{0.5}TiO_3$-related materials close to the MPB [12–16].

In order to enhance some of the physical properties, great attention has been dedicated to modified PZT-based ceramics, where the stability of ferroelectric phase is strongly affected by chemical substitutions of lead ions at the A-site as well as at the B-site by controlling the Zr/Ti ratio. In particular, lanthanum (La^{3+}) ion is a common substitutional cation mostly used on dodecahedral sites, leading to high performance of the La-modified PZT (PLZT) system [8]. For instance, PLZT system shows lower coercive electric field as well as both higher dielectric permittivity and optical transparency, when compared to the pure PZT material, providing additional insight for possible transducer, electrostrictive and electro-optic devices [17]. However, in order to obtain high density samples, it is required very high sintering temperature (around 1000–1300 ^oC) [18].

It is well known that lead (Pb^{2+}) ions severely evaporate during the sintering treatment in PZT-based ceramics, which contributes for the formation of undesired pyrochlore phases and significantly affects the physical and chemical properties of the samples. The role of intrinsic charge-defects generated during the synthesis process affects significantly the microstructural properties and, therefore, it cannot be ignored. During the thermal treatment of the samples at very high temperatures, the different crystallization mechanisms of both pyrochlore ($A_2B_2O_7$) and perovskite phases result in discordant grain-boundaries between the two phases, which could contribute to the current leakage through the interface between both phases in the material. The obtaining process of PLZT could promote the formation of small amounts of pyrochlore phases, such as $La_2(Zr,Ti)_2O_7$ and $Pb_2(Zr,Ti)_2O_7$, all with cubic symmetry structure (F*d*-3*m* space group) [19]. On the other hand, the formation of these defects causes lattice distortions in the ABO_3 perovskite structure. Since the lattice distortions and domain switching contribute to the piezoelectric response [10], the pyrochlore-related defects will affect the electrical, dielectric and mechanical performance of the materials. In this context, pyrochlore-free materials are extremely important for the design of high-performance piezoelectric devices. Therefore, the investigation of the influence of these minority phases on the structural, electrical and ferroelectric properties is essential in order to understand the dynamics of the involved defect mechanisms on PZT-based compounds. A way to compensate the appearance of the minor secondary phase can be avoided using an excess of volatile lead precursor. Lead deficiency in the bulk ceramics results in lead-vacancies while lead-excess is accommodated by forming octahedral site-vacancies. The aim of the present work is to investigate the influence of the Pb-excess on the ferroelectric phase stabilization of the lanthanum-modified lead zirconate titanate system, $Pb_{1-x}La_x(Zr_{1-y}Ti_y)_{1-(x/4)}O_3$ (PLZT). In particular, the influence on the structural characteristic as well as its correlations with the microstructural and ferroelectric properties has been analyzed. According to the phase diagram for the PLZT system, reported by Haertling [11], the Zr/Ti ratio for the $Pb_{0.94}La_{0.06}(Zr_{0.6895}Ti_{0.2955})O_3$ composition reveals the better performance for piezoelectric applications for materials with rhombohedral symmetry, which possesses a relatively high solubility of the La^{3+} ions (~12% mol) and has been indeed scarcely explored in the literature in view of their structrural characteristics. In this way, in order to control the lead excess in other compositions considering different La ions amount, we have fixed in this work the lanthanum concentration in x = 0.06, since it belongs to the compositions with relatively low phase transition temperature (< 400 ^oC), and without the well-known relaxor effect. Such relaxor characteristic of the phase transition, which manifests as a very strong frequency dispersion of the dielectric parameters, could directly affect the physical properties to be investigated.

II. Experimental procedure

$Pb_{0.94}La_{0.06}(Zr_{0.6895}Ti_{0.2955})O_3$ ceramics were prepared by a conventional solid state reaction process, considering 0, 2, 5, 10, 15 and 20 mol% PbO-excess in order to compensate the high volatility of this cation during the high-temperature annealing step. High purity reagents, PbO (99%, Vetec), TiO_2 (98%, Vetec), ZrO_2 (99%, Aldrich) and La_2O_3 (99.9%, J. T. Baker), were used as starting chemical precursors. The raw materials were mixed and then ball-milled for 12 h. The powders were dried and then prefired (calcinated) at 850 °C for 3.5 h in air atmosphere. The powders were milled again and a second calcination process was carried out at 1100 °C for 3.5 h. The powders were subsequently ball-milled for 2 h, dried and then uniaxially and isostatically pressed at 13 MPa and 350 MPa, respectively. Finally, the samples were sintered in an air atmosphere at 1250 °C for 2 h. The structural properties were investigated on powdered ceramic samples from the X-ray diffraction (XRD) technique using a Shimadzu XRD-6000 diffractometer with CuKα radiation. The measurements were performed at room temperature in the 2θ range of 10–130° considering a fixed counting time and a scan-step of 0.02°. The Rietveld refinement method has been employed in order to calculate the different structural parameters with the help of the GSAS software package [20]. Additionally, Raman spectroscopy was investigated, also at room temperature, by using a micro-Raman spectrometer (Horiba Jobin Yvon LabRam HR Evolution), with the laser source of 532 nm wavelength. The microstructural properties were analyzed by scanning electron microscopy (SEM) using a Vega3 Tescan microscope. The SEM micrographs were performed on fractured polycrystalline ceramics. The density of the samples was measured from the Archimedes' method, using an analytical Shimatzu AYU220 scale. To obtain the electrical characterizations, electric contacts were applied on both parallel surfaces of the pellets, using conducting silver paste fired at 590 °C. The ferroelectric properties were investigated from the polarization versus electric field (*P–E*) hysteresis curves, obtained at 1 Hz and room temperature, using modified Sawyer-Tower circuit. Additional information concerning the circuit diagram and experimental set-up can be found elsewhere [21]. The samples are hereafter labeled as PLZT 6/70/30_*x*, where *x* represents the PbO-excess content (*x* = 2, 5, 10, 15 and 20 %).

III. Results and discussion

III.1 XRD analysis

Figure 2 shows the X-ray diffraction patterns of the studied PLZT 6/70/30_*x* compositions, obtained at room temperature. The results revealed that the ferroelectric perovskite phase was successfully obtained for all the samples and there is no significant change in crystal structure due to the modification of the PbO-excess. A detailed inspection of the experimental profiles revealed the splitting of the (003) and (021) reflections around the 2θ range of 38.0–39.5°, as well as a single peak, corresponding to the (202) reflection around 44.5° for all the ceramics.

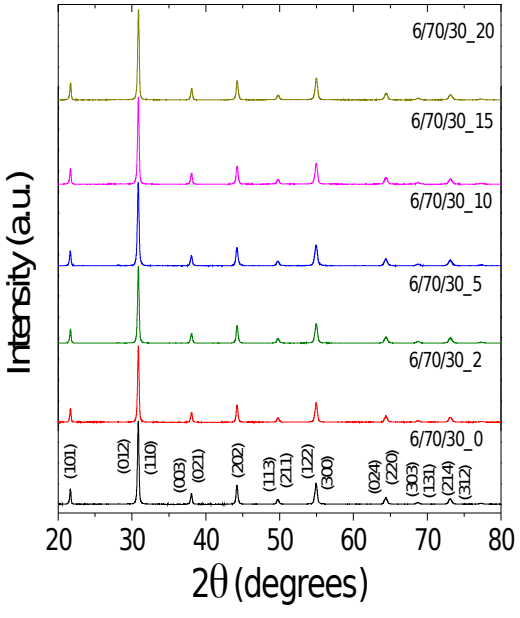

Figure 2: X-ray diffraction patterns obtained at room temperature for the studied compositions. The indexation of the diffraction peaks is the same for all the samples

This result is a typical characteristic of rhombohedral symmetry structures [22]. Taken

into account these characteristics, the diffraction peaks are indexed according to the ICSD–54894 database corresponding to a non-centrosymmetric space group R3*m* (SPG No. 160) [23].

For a better examination of the structural properties, the XRD patterns have been expanded in the 2θ range of 26–32°, as shown in the Figure 3. A relative lower peak corresponding to a secondary phase, marked with symbol (*), has been observed around 28.12° for the 6/70/30_0, 6/70/30_2, 6/70/30_5 and 6/70/30_10 compositions, which has been identified as the Pb_2O_3 phase (P*mnb* space group, ICSD–36275) [24]. The unit-cell parameters (*a*, *b*, *c*) and volume (*V*) reported for this phase are: *a* = 3.898(2) Å, *b* = 6.441(3) Å, *c* = 7.679(4) Å and *V* = 192.80 Å^3 [24]. However, for the higher PbO-excess content (15 and 20 mol %), the peak associated to the Pb_2O_3 phase disappears and there is no obvious change in the perovskite phase structural characteristics.

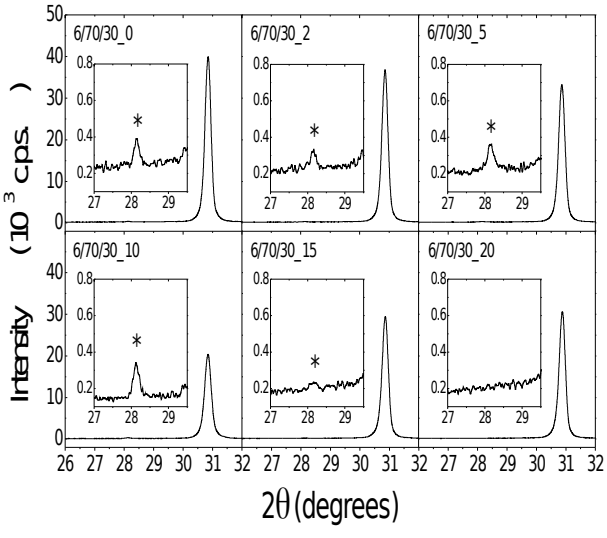

Figure 3: Expanded XRD patterns in the 2θ range between 26 and 32° for the studied compositions. The peak marked with an asterisk is assigned to the secondary Pb_2O_3 phase

A detailed analysis of the structural properties has been performed by the Rietveld refinement, considering a two-phases model (perovskite and Pb_2O_3). In the Rietveld method, the last-squares refinements are carried out until the best fit is obtained

between observed diffraction pattern and “calculated” pattern, based on both crystal structure(s) and instrumental parameters [25]. The refinement has been performed here taking into account the incorporation of the lanthanum ions at the *A*-site of the perovskite structure, starting with the nominal composition showed in the experimental procedure section. The atomic coordinates in the asymmetric unit-cell were assumed as Pb/La at ($x_{Pb/Ti}$, $x_{Pb/Ti}$, $x_{Pb/Ti}$) coordinates, Ti/Zr at ($x_{Ti/Zr}$, $x_{Ti/Zr}$, $x_{Ti/Zr}$) and the O(I) positions at ($x_{O(I)}$, 0, 0). The initial positions are taken from the Inorganic Crystal Structure Database [24] considering a rhombohedral crystallographic basis. The initial occupation factors were assumed considering the formation of lead vacancy, which are introduced into the structure by the replacement of Pb^{2+} by La^{3+} ions. The *A*-site (*B*-site) occupancy was shared between Pb and La atoms (Ti and Zr atoms). The initial structural model for the calculation of the diffraction patterns corresponds to both the perovskite and pyrochlore phases. The characteristic of the structural parameters for the Pb_2O_3 has been taken from the ICSD–36275 database [24], as aforementioned. The obtained results are shown in the Figure 4 for the 6/70/30_10 composition, as an example of the obtained refinement results for the other samples.

The observed data are indicated with symbol, while the corresponding calculated profiles are represented by a solid line. The vertical marks below the pattern represent the positions of the Bragg’s reflections for both phases. The difference between the observed and the calculated data is plotted at the bottom of the figure, showing a good agreement between the experimental and the theoretical results. The structural parameter, such as refined unit-cell volume (*V*) as well as the weight percent's (%) of each phase (perovskite and Pb_2O_3), are given in the Table 1 for all the compositions. The refinement structural parameters, such as the goodness-of-fit (χ^2) as well as the residual and weighted residual profile R-factors (R_p and R_{wp}), respectively, are also reported. Values of R_p and R_{wp} lower than 10-12 %, with the corresponding correct solution, are acceptable for an excellent refinement [26].

The obtained results show a slight variation of the structural parameters (*a* and *α*) and reveal a non-tendency with the increase of PbO-excess. As can be seen in the Table 1, a slight contraction of the unit-cell volume is observed for all samples considering PbO-excess, with respect to the pure PLZT 6/70/30_0 ceramic.

On the other hand, the phase percentage of R3*m* is higher than 98% for all studied systems. A considerable increase of the weight percent for Pb_2O_3 phase is obtained in the PLZT 6/70/30_10 composition, when compared to the samples with smaller PbO-excess.

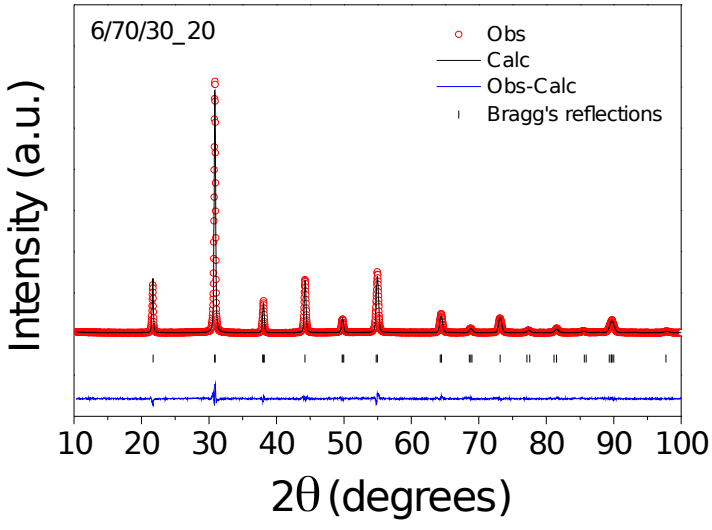

Figure 4: Rietveld refinement of the X-ray diffraction patterns for the 6/70/30_20 composition. The experimental patterns (open circle), the calculated profiles (black solid line), and the difference between them (bottom blue solid line) and the Bragg's positions (vertical lines) are also shown.

Table 1 : Unit-cell volume (*V*), weight percent (%) for both perovskite and Pb_2O_3 phases and the refinement parameters (R_p, R_{wp} and χ^2) for the studied compositions.

Sample	*V* (Å^3)	Weight percent (%)		Goodness factors		
		Perovskite	Pb_2O_3	R_{wp} (%)	R_p (%)	χ^2
6/70/30_0	68.43(4)	99.40	0.60	7.8	6.5	2.0
6/70/30_2	68.35(5)	99.60	0.40	8.8	7.3	2.2
6/70/30_5	68.37(2)	99.56	0.44	11.1	8.4	3.3
6/70/30_10	68.36(4)	98.70	1.30	7.8	6.6	2.9
6/70/30_15	68.31(7)	100	–	8.4	6.8	1.7
6/70/30_20	68.32(8)	100	–	8.2	6.7	1.7

In addition, the obtained R_{wp} and R_p factors are close to the 10%, which confirms that the refinement process is reliable. The very low values obtained for the χ^2 parameter also confirm the good agreement between the calculated and experimental patterns, thus supporting the quality of the refinement process.

III.2 Raman spectroscopy analysis

In order to identify in more details the evolution of the crystal structure as a function of PbO-excess, Raman spectra were performed at room temperature for the studied ceramics. Figure 5 shows the obtained results for all the compositions, which reveal similar spectra to those obtained for others lead-based bulk ceramics [27].

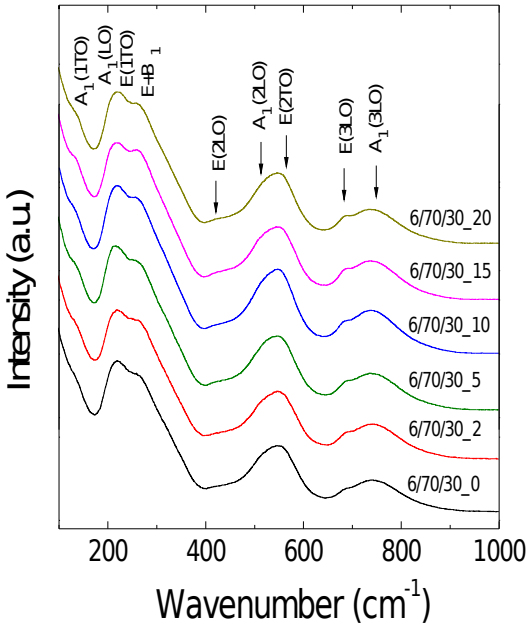

Figure 5: Room temperature Raman spectra for different PbO-excess contents. The indexation of the vibration modes is the same for all the samples.

These results confirm that the perovskite phase, previously identified by XRD analysis, was successfully obtained in the studied system. As can be observed, no drastic changes of the Raman spectra are observed with the increase of PbO-excess content. For the Raman activity to takes place, a change in the polarizability of the material during the interaction with the radiation should be observed [28]. The vibrational modes in a molecule can be classified according to the number and type of the symmetry elements, which remain invariant during vibration. These modes can by symmetric (i.e. the A1 mode) or anti-symmetric (i.e. the E mode). Due to the long-range electrostatic force existing in the material the A1 and E vibrational modes show longitudinal (LO) and transversal (TO) optical components. In this way, further information from the fundamental point of view can be obtained from the literature [28].

According to the group theory, 13 Raman active modes are expected for the rhombohedral (R3*m*) ferroelectric phase [29]; (Z = 2): $\Gamma_{Raman} = 7A_1 + 6E$. However, the individual Raman modes are unable to be observed due to their overlapping. The analyzed wavenumber range (70–1000 cm^{-1}) can be separated into three regions, which have been labeled as: *i)* low wavenumbers, ≤ 350 cm^{-1} (region I); *ii)* middle wavenumbers, 350–600 cm^{-1} (region II); and *iii)* high wavenumbers, ≥ 600 cm^{-1} (region III), as indicated in the Figure 6.

In general, the interpretation of the Raman spectra obtained for disordered solid-solutions can be difficult because the spectrum could develop an overlapping of the vibration modes in the same spectral region. In that case, it is common to adopt an alternative mathematical procedure, which allows the identification of the characteristic peaks as well as the presence of shoulders [30]. Therefore, in order to analyze in details the observed results in Figure 5, the number of the spectral components was estimated by a standard fitting method previously reported by Buixadeiras et al. [30], which is based on the location of the curvature maxima in concave-down (CMCD) spectral regions of the recorded Raman spectra.

For the studied samples, all the Raman spectra revealed 9 active vibrational modes, which have been associated in the Figure 5 with the Rhombohedral (R3*m*) phase, according to the reported results for the PZT-based system [29]. The indexation of the vibrational modes is the same for all the compositions. The peak position for each Raman active mode (natural wavenumber, cm^{-1}) has been obtained by the CMCD method and the results are shown in the Figure 6, for all studied samples, as function of the PbO-excess.

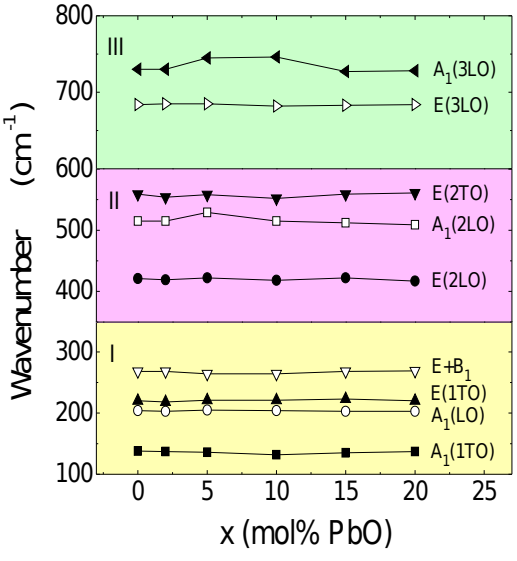

Figure 6: PbO-excess concentration (*x*) dependence of the wavenumber, showing the Raman active modes, divided into three regions according to the wavenumber values: region I (≤ 350 cm^{-1}), region II (350–600 cm^{-1}) and region III (≥ 600 cm^{-1}).

As can be observed, the variation of the wavenumber is affected for some modes into the ABO_3 perovskite structure, which confirms the variation of local symmetries of the structure due to the concentration of the PbO-excess. In the region I, for wavenumber below 350 cm^{-1}, no compositional dependence of the A_1(1TO) mode is observed for the studied ceramics. On the other hand, the wavenumber of the A_1(LO), E(1TO) and E + B_1 modes observed around 204, 220 and 268 cm^{-1}, respectively, remains almost constant with the increase of PbO-excess content. Similar behavior is also observed for the E(2LO) and E(2TO) modes in the region II (350–600 cm^{-1}), as well as in E(3LO) mode, at 684 cm^{-1}, in the region III (≥ 600 cm^{-1}), showing no dependence with the PbO-excess concentration for all the analyzed compositions. In this region III, however, an increase of the last A_1(3LO) mode from around 730 cm^{-1}, for the PLZT 6/70/30_0 sample, up to 746 cm^{-1}, for the PLZT 6/70/30_10 composition, is obtained; it decreases again considerably for higher PbO-excess concentrations (15 and 20 mol %). This mode has been previously associated in the literature with the B–O stretching vibrations in PZT-type perovskites [31]. The B-O stretching vibration mode of the BO_6 octahedra in the perovskite structure is schematically illustrated in the Figure 7 [32]. For the PLZT system, the *A*-site (*B*-site) is occupied by the La and Pb (Zr and Ti) ions.

The representation is displayed considering the unit-cell with unit formula number equal to 1 (Z = 1).

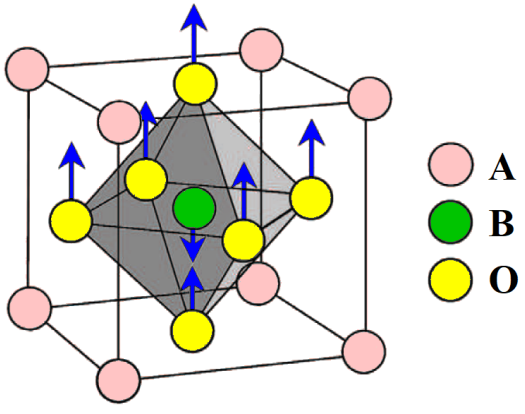

Figure 7: Schematic illustration of the B-O stretching mode in the perovskite structure, representing the A and B sites and oxygen (O) ions [32, 33].

Similar behavior is also observed for the A_1(2LO) mode in the region II, which has been associated to the O–B–O bending vibrations [31]. An schematic illustration for this mode is presented in Figure 8 [34], representing the O-Zr/Ti-O bending vibration mode along the *a*, *b* and *c*-axes. The example is showed for tetragonal phase of the PLZT system with Z = 1, where the spontaneous polarization is along the [001] crystallographic direction.

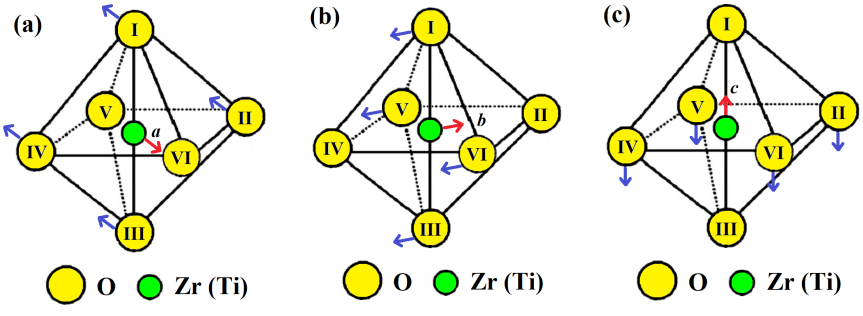

Figure 8: Schematic illustration of the O-Zr/Ti-O bending mode along (a) *a*-axes, (b) *b*-axes and (c) *c*-axes, for the tetragonal phase of the PLZT [34].

In this case, a shift to a higher Raman wavenumber, from 515 cm^{-1} to 529 cm^{-1} is found as the PbO-excess content increases up to 5 mol%, and then decrease with the

increase of the PbO-excess concentration. The shift to a higher wavenumber suggests an increase of the force constant of the O–B–O bonding. Thus, a shortening of the O–B–O bond distance and, therefore, a strengthening of the O–B–O vibration is expected. For the samples with x = 10, 15 and 20 mol% PbO, a decrease in the wavenumber results in the weakening of the O–B–O vibration of the A_1(2LO) mode with the increase of the PbO-excess content.

III.3 Microstructural analysis

Scanning electron microscopy was used in order to investigate the microstructure of the samples, such as morphology and average grain-size as well as the presence of liquid phase as a function of the lead excess. SEM micrographs for the studied ceramics are shown in the Figure 9. The results revealed homogeneous microstructure with both uniform and well-defined grains for all samples.

The average grain-size (Φ) was determined by the linear intercept method from the SEM images and the obtained values are shown in the Table 2 for all analyzed compositions. A tendency to a decrease in the Φ parameter is observed with the increase of the PbO-excess content. This decrease could be associated with the presence of liquid phase in the grain boundary region, which is formed during the sintering process and seems to be more prominent for the lower PbO-excess concentrations. The formation of the liquid phase allows more effective mass transport, which promotes the diffusion of the elements in the solid solutions, leading to an anomalous growth of the average grain-size.

Table 2 : Values of the average grain-size (Φ) as well as apparent (ρ_A), theoretical (ρ_T) and relative (ρ_R) densities for the studied compositions.

Sample	Φ (μm)	ρ_A (g/cm^3)	ρ_T (g/cm^3)	ρ_R (%)
6/70/30_0	2.16 ± 0.24	7.5472	7.9708	94.7
6/70/30_2	2.02 ± 0.20	7.6532	7.9771	95.9
6/70/30_5	1.75 ± 0.23	7.5372	7.9757	94.5
6/70/30_10	1.91 ± 0.32	7.5737	7.9886	94.8
6/70/30_15	1.69 ± 0.14	7.7303	7.9760	96.9
6/70/30_20	1.65 ± 0.17	7.5762	7.9747	95.0

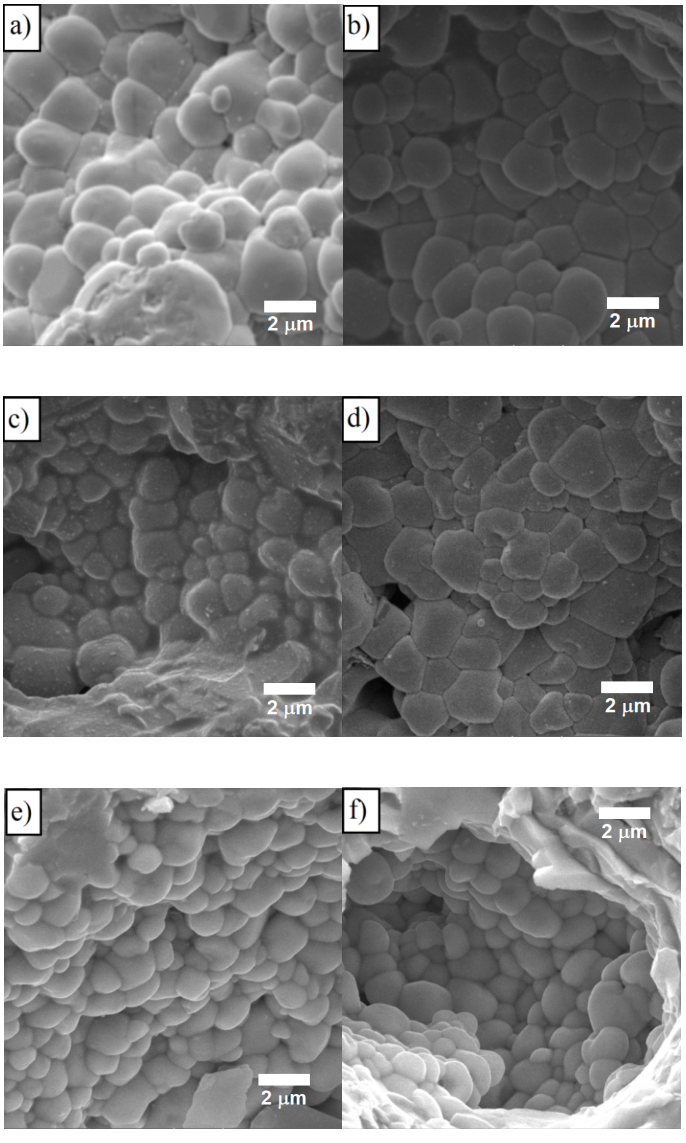

Figure 9: Scanning electron microscopy micrographs for the PLZT 6/70/30_0 (a), PLZT 6/70/30_2 (b), PLZT 6/70/30_5 (c), PLZT 6/70/30_10 (d), PLZT 6/70/30_15 (e) and PLZT 6/70/30_20 (f) compositions.

The theoretical density (ρ_T) was calculated from the values of the structural parameters obtained from the refinement.

In order to quantify the density of the studied ceramics, the apparent density (ρ_A) has been obtained from the Archimedes' method and, hence, compared with the ρ_T value for each composition. The obtained values for ρ_A, ρ_T and the relative density (ρ_R) are also shown in the Table 2. High relative density values (> 94%) are obtained for all the samples, thus suggesting low porosity levels as shown in the SEM micrograph. The obtained result for these materials shows to be higher than the reported for other lead-based ceramic systems [35, 36]. The high ρ_R values for the studied ceramics could be associated to the reaction kinetics in the sintering process when considering PbO-excess [37].

III.4 Ferroelectric properties

The hysteresis loops (*P–E* curves) were performed at room temperature in order to analyze the influence of PbO-excess in the ferroelectric response. Figure 10 shows the *P–E* curves for all studied compositions. Well-defined hysteresis loops, typical for ferroelectric systems, have been obtained for all samples. Other important parameters such as saturation polarization (P_S), which represents the maximum polarization of the material when all the dipoles are oriented along the same direction of the applied electric field and the coercive field (E_C), representing the strength of the electric field necessary to reduce the polarization to zero, can be also extracted from the hysteresis loops. These parameters, together with P_R, were obtained from the *P-E* curves of Figure 10 and are shown in the Table 3. It can be seen that the remnant (P_R) and saturation (P_S) polarization values as well as the coercive field (E_C) are affected by the concentration of PbO-excess.

As observed, there is no a monotonous variation in the P_R, P_S and E_C values with the increase of the PbO-excess concentration. Both P_R and P_S parameters for the PLZT 6/70/30_10 composition are clearly lowered when compared to the other studied compositions. As aforementioned, a highest weight percent of the undesirable Pb_2O_3 phase (~1.30 %) was revealed by the XRD results for this sample. Therefore, the decrease of these parameters (P_R and P_S) could be associated to the inability of the switching process of the ferroelectric domains as a result of the high percentage of the secondary phase detected for the PLZT 6/70/30_10 sample. A secondary phase of Pb_2O_3 can act as pinning centers for the ferroelectric domain walls, which results in the drawback of the domains reversal process.

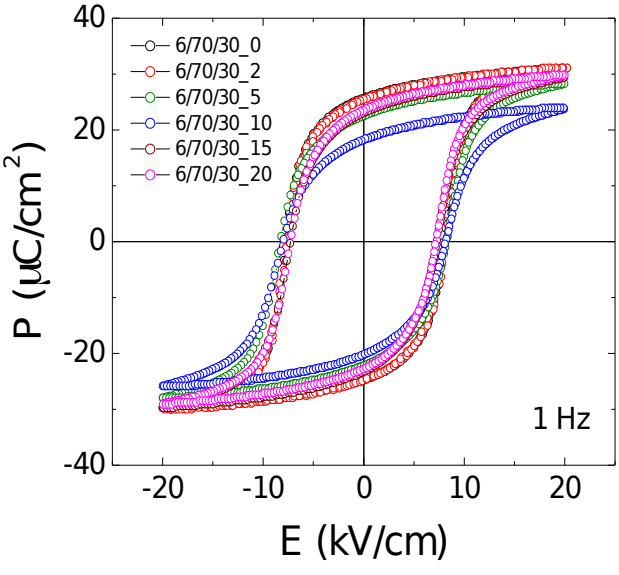

Figure 10: Hysteresis loops for the studied compositions, obtained at room temperature and 1 Hz.

Table 3 : Values of the remnant polarization (P_R), saturation polarization (P_S) and coercive field (E_C) for the studied compositions.

Sample	P_R (μC/cm²)	P_S (μC/cm²)	E_C (kV/cm)
6/70/30_0	26	31	7.7
6/70/30_2	25	31	7.7
6/70/30_5	22	28	8.2
6/70/30_10	18	24	7.8
6/70/30_15	23	29	7.4
6/70/30_20	23	30	7.4

IV. Conclusion

Solid-state reaction sintering process has been used to prepare lead lanthanum zirconate titanate (PLZT 6/70/30) ceramics with different PbO-excess content, which is usually added in order compensate the charge unbalance, thus leading to an enhance in the densification of the studied lead-based compositions. The structural, microstructural and electrical properties, as examined by XRD, Raman, SEM and hysteresis loops, revealed to be dependent on the PbO-excess concentration. It was determined that a 15 mol% PbO-excess was required to obtain PLZT bulk ceramics without secondary Pb_2O_3 pyrochlore phase. High relative density values (>94 %) suggest highly dense microstructures for all studied ceramics, which have been related to the kinetics during the synthesis of the samples with the inclusion of PbO-excess. The results of the Raman spectra showed that the structural properties were affected by the excess of PbO, revealing a shifting of the wavenumber for some active vibrational modes. A decrease in both remnant and saturation polarization values is revealed with the addition of 10 mol % PbO-excess, which lead to a reduction of the long-range interaction for this composition.

Acknowledgements: The authors would like to thank the financial support from the National Council of Scientific and Technological Development (CNPq) under grant 303314/2016-8, Minas Gerais Research Foundation (FAPEMIG) under grants PPM-00661-16 and APQ-02875-18 and Coordenação de Aperfeiçoamento de Pessoal de Nível Superior - Brasil (CAPES) - Finance Code 001 Brazilian agencies.

Complementary informations on authors:

e-mail: santos@ufu.br, ORCID: 0000-0002-7906-4343, Web of Science ResearcherID: C-5823-2013, Scopus Author ID: 23488953000, Research Gate: Jose_De_Los_Santos_Guerra

Cite this paper: A.C. Silva, Y. Mendez-González, E.C. Lima, J.D.S. Guerra, OAJ Materials and Devices, vol 5(2) – chap No13 in "*Perovskites and other Framework Structure Crystalline Materials", p405* (Coll. Acad. 2021) – DOI:10.23647/ca.md20201806

REFERENCES

1. K.Uchino, *Ferroelectric Devices*, Marcell Dekker Inc., New York (2000)
2. B.Jaffe, W.R.Cook, H.Jaffe, *Piezoelectric Ceramics*, Academic Press, London-New York (1971)
3. B.Jaffe, R.S.Roth, S.Marzullo, *J. Appl. Phys.*, **vol.25**, p 809 (1954)
4. K.Kakewaga, O.Matsunaga, T.Kat, Y. Sasaki, *J. Am. Ceram. Soc.*, **vol.78**, p 1071 (1995)
5. J.C.Fernandes, D.A.Hall, M.R.Cockburn, G.N.Greaves, *Nucl. Instrum. Methods Phys. Res. B*, **vol.97**, p 137 (1995)
6. M.Hammer, C.Montry, A.Endriss, M.J.Hoffmann, *J. Am. Ceram. Soc.*, **vol.81**, p 721 (1998)
7. A.P.Wilkinson, J.Xu, S.Pattanaik, J.L.Billinge, *Chem. Mater.*, **vol.10**, p 3611 (1998)
8. Y.Xu, *Ferroelectric materials and their applications*, Elsevier Science Publishers BV, Amsterdam (1991)
9. A. M.Glazer, *Acta Crystallogr. A*, **vol.31**, p. 756 (1975)
10. W.Heywang, K.Lubitz, W.Wersing, *Piezoelectricity, Evolution and Future of a Technology*, Springer Series in Material Science, Berlin (2008)
11. G.H.Haertling, *J. Am. Ceram. Soc.*, **vol.82**, p 797 (1999)
12. L. Egerton, D.M.Dillon, *J. Am. Ceram. Soc.*, **vol.42**, p 438 (1959)
13. C.Xu, D.Lin, K.W.Kwok, *Solid State Sci.*, **vol.10**, p 934 (2008)
14. Y. Guo, Y. Liu, R.L. Withers, F. Brink, H. Chen, *Chem. Mater.*, **vol.23**, p 219 (2011)
15. P.K.Panda, B.Sahoo, *Ferroelectrics*, **vol.474**, p 128 (2015)
16. R.R.McQuade, M.R.Dolgos, *J. Solid State Chem.*, **vol.242**, p 140 (2016)
17. R.G.Sabat, *Characterization of PLZT Ceramics for Optical Sensor and Actuator Devices*, *Ceramic Materials - Progress in Modern Ceramics*, Prof. Feng Shi (Ed.), London (2012)
18. P.Goel, S.Sharma, K.L.Yadav, A.R.James, *Pramana – J. Phys.*, **vol.65**, p 1127 (2005)
19. Inorganic Crystal Structure Database - ICSD, FIZ Karlsruhe, Germany (2014)
20. A.C.Larson, R.B.Von Dreele, *General Structure Analysis System (GSAS)*, Los Alamos National Laboratory Report LAUR 86-748 (2000)
21. C.B.Sawyer, C.H.Tower, *Phys. Rev.*, **vol.35**, p 269 (1930)
22. P.Zavalij, V.K.Pecharsky. Fundamentals of Powder Diffraction and Structural Characterization of Materials, Srpinger, New York (2005)
23. V.V.Efimov, S.S.Khasanov, B.N.Mavrin, N.N.Novikova, A.V.Shilnikov, A.I.Burkhanov, V.V.Sikolenko, A. Sternberg, S.I.Tiutiunnikov, D.M.Többens, V.A.Yakovlev, *Ferroelectrics*, **vol.302**, p 327 (2004)
24. A. Bystroem, *Mineralogi och Geologi*, **vol.24**, p 1 (1947)

25. R.A.Young, The Rietveld Method (IUCr Oxford University Press, New York, 1993)
26. B.H.Toby, *Powder Diffract.*, **vol.21**, p 67 (2006)
27. E.Buixaderas, M.Berta, L.Kozielski, I.Gregora, *Phase Transit.*, **vol.84**, p 528 (2011)
28. K.Nakamoto, *Infrared and Raman Spectra of Inorganic and Coordination Compounds*, John Wiley & Sons, New Jersey (2009)
29. M.Deluca, H.Fukuruma, N.Tonari, C.Capiani, N.Hasuike, K.Kisoda, C.Galassi, H.Harima, *J. Raman Spectrosc*., **vol.42**, p 488 (2011)
30. E.Buixaderas, I.Gregora, M.Savinov, J.Hlinka, L.Jin, D.Damjanovic, B.Malic, *Phys. Rev. B*, **vol.91**, 014104 (2015)
31. M.-K.Zhu, P.-X.Lu, Y.-D.Hou, X.-M.Song, H.Wang, H.Yan, *J. Am. Ceram. Soc.*, **vol.89**, p 3739 (2006)
32. E.B. Araújo, *Recent Advances in Processing, Structural and Dielectric Properties of PMN-PT Ferroelectric Ceramics at Compositions Around the MPB*, Advances in Ceramics - Electric and Magnetic Ceramics, Bioceramics, Ceramics and Environment, Costas Sikalidis, IntechOpen (2011) DOI: 10.5772/18083
33. R.Ashiri, *Vib. Spectrosc.*, **vol.66**, p 24 (2013)
34. Y.Zhang, X.Cheng, S.Zhang, *Appl. Phys. A*, **vol.89**, p 685 (2007)
35. C.Sangsubun, A.Watcharapasorn, S.Jiansirisomboon, *Integr. Ferroelectr.*, **vol.149**, p 61 (2013)
36. L.Hai, Z.Bo-Ping, P.Yu, Z.Lei, W.Kai-sheng, L.Yan-tao, *J. Mat. Res.*, **vol.30**, p 782 (2015)
37. L.Zhou, A.Zimmermann, Y.P.Zeng, F.Aldinger, *J. Mat. Sci.*, vol.15, p 145 (2004)